Journal of Magnetic Resonance **153,** 32–47 (2001)
doi:10.1006/jmre.2001.2422, available online at http://www.idealibrary.com on IDEAL®

Cross-Correlated ^{19}F Relaxation Measurements for the Study of Fluorinated Ligand–Receptor Interactions

Jeffrey W. Peng

Protein NMR Group, Vertex Pharmaceuticals, Inc., 130 Waverly Street, Cambridge, Massachusetts 02139-4242

E-mail: jeffrey_peng@vpharm.com

Received March 13, 2001; revised July 30, 2001; published online October 5, 2001

Fluorine is often used in drug-design efforts to enhance the pharmacokinetic properties of biologically active compounds. Additionally fluorine nuclei (^{19}F) have properties that are well suited to current pharmaceutical NMR screening programs. Together, these considerations have motivated our interest in the utility of fluorine relaxation parameters to study ligand–receptor interactions. Here, we investigate the potential for cross-correlated relaxation effects between the ^{19}F anisotropic chemical-shift and ^{19}F–^{1}H dipole–dipole relaxation mechanisms to help pinpoint and quantify exchange processes. Methods are proposed and demonstrated in which the magnitude ratio of the transverse cross-correlation rate constant η_{xy} and the fluorine transverse relaxation rate constant, R_2, help estimate the exchange rate constant for ligand-binding equilibria. These exchange rate constants provide estimates of the ligand dissociation rate constants k_{off} and can thus provide a means for rank-ordering the binding affinities of ligands identified in pharmaceutical screens.

Key Words: **relaxation; fluorine; screening; binding; cross-correlation.**

I. INTRODUCTION

Nuclear magnetic resonance (NMR) spectroscopy is becoming increasingly valued as a screening tool for lead generation in pharmaceutical drug discovery programs. In response, NMR spectroscopists have intensified their efforts toward optimizing and developing strategies capable of identifying and characterizing receptor–ligand interactions (*1*). A large subset of the current strategies screen compound libraries by looking for perturbations (e.g., line broadening, chemical shift changes) in the NMR spectra of the compounds upon the addition of a receptor. These strategies are dominated by proton (^{1}H) NMR methods. However, fluorine NMR (^{19}F) methods offer some unique advantages that merit consideration. First, the absence of endogenous fluorine in proteins and nucleic acids means that ^{19}F NMR yields automatically ligand-selective observation. Secondly, the chemical shift range of fluorine is much larger than the proton shift range, ≈900 ppm (*2*), thus increasing the likelihood of well-resolved lines. This also means that the fluorine chemical shift is much more sensitive to local environmental effects, which translates into both larger binding-induced chemical shift perturbations and exchange-induced line broadening. Thirdly, the favorable pharmacokinetic properties of fluorinated ligands have already established ^{19}F as a standard component in medicinal chemistry's "toolkit"; this contrasts with ^{13}C or ^{15}N, for which difficulties with synthesis or high cost often precludes their incorporation into nonpeptide ligands. Finally, ^{19}F occurs at 100% natural abundance and has a gyromagnetic ratio that is competitive with ^{1}H. Given these assets, a scrutiny of ^{19}F NMR parameters for their binding information content is of considerable interest for receptor–ligand studies.

NMR relaxation experiments can provide information concerning ligand-binding affinities. In particular, measurements of the spin–lattice relaxation rate in the rotating frame ($R_{1\rho}$) can elucidate the rate constants governing rapid chemical exchange processes (*3, 4*). The resulting exchange rate constants can then give estimates of the corresponding K_D values, thus providing measures of binding affinity. However, obtaining accurate exchange rate constants can be difficult if the nonexchange versus exchange contributions to $R_{1\rho}$ cannot be distinguished from one another. This is often the case for the weakly binding ligands identified by NMR-based screening methods. Here, we propose methods for alleviating this difficulty for fluorinated ligands through the measurement of transverse cross-correlated ^{19}F relaxation measurements. When combined with the more standard transverse relaxation measurements, they permit the separate estimation of the nonexchange contributions, thus allowing for a more accurate definition of the exchange rate constant. Knowledge of the exchange rate constant gives one the ability to estimate the corresponding equilibrium dissociation constant, K_D, which is a measure of ligand-binding affinity.

Previous ^{19}F studies aimed at ligand–receptor interactions have used chemical shift perturbations and relaxation experiments in both fluorinated proteins or ligands. The relaxation measurements have consisted of either standard auto-relaxation measurements (i.e., $R_1 = 1/T_1$, $R_2 = 1/T_2$, and $R_{1\rho} = 1/T_{1\rho}$) or heteronuclear ^{19}F–^{1}H NOE measurements (see, e.g., (*2, 5–10*)). However, studies of cross-correlated fluorine relaxation have been fewer and restricted mainly to theoretical analyses

1090-7807/01 $35.00

(*11–13*). Accordingly, the studies presented here focus on both the theory and measurement of cross-correlated fluorine relaxation in the context of their potential benefits toward the elucidation of ligand–binding affinities. Thus, these studies directly address the growing need for methods that can estimate and compare the binding affinities of ligands generated in NMR-based pharmaceutical screening.

In what follows, we present pulse schemes that detect and measure transverse ^{19}F–^{1}H CSA-DD interference effects. We then apply these schemes in combination with fluorine $R_{1\rho}$ measurements to estimate the dissociation rate constant (k_{off}) and the equilibrium dissociation constant (K_{D}) of a small singly fluorinated aromatic compound that binds reversibly to a 15,400-Da protein target.

II. THEORY

(i) Cross-correlation between the ^{19}F–^{1}H dipole–dipole and ^{19}F chemical shift anisotropy relaxation mechanisms. We are interested in the relaxation interference effects, or, cross-correlation between a ^{19}F–^{1}H dipole–dipole (DD) interaction, and the chemical shift anisotropy (CSA) of the ^{19}F nucleus. To investigate these effects, we focus on the ^{19}F relaxation properties of the singly fluorinated aromatic ring schematized in Fig. 1. This moiety is a common fragment in "drug-like" molecules (*14*). The fluorine NMR spectrum is a quartet defined by scalar couplings to the *ortho* proton ($J_{\text{FI}} \approx 12$ Hz) and to the remote S proton ($J_{\text{FS}} \approx 8.6$ Hz). The dominant ^{19}F–^{1}H DD interaction is with the *ortho* proton I. Additional DD interactions with other ring protons are negligible on account of the greater fluorine–proton distances involved. Thus, in what follows, "DD" refers specifically to the dipole–dipole interaction between the fluorine and the *ortho* proton I unless otherwise stated. Similarly, the "CSA" interaction is understood to be that of the fluorine nucleus.

Thorough presentations of the fundamental theory of relaxation interference effects are abundant in the literature (*15–21*). The presence of these effects in ^{19}F NMR spectra have been discussed by several groups (*11–13, 22*). Our focus here is to expound on those theoretical aspects of the fluorine CSA-DD interference effects relevant for ligand-binding studies.

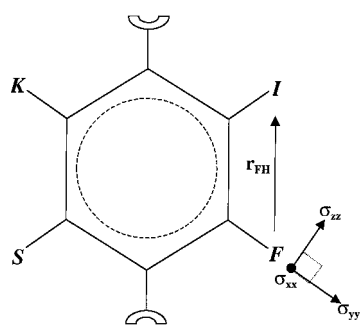

FIG. 1. Schematic of the aromatic fluorine moiety used in this study. "F" denotes the fluorine nucleus, while "I," "S," and "K" denote protons. The semicircles indicate connections to other chemical groups (typically aromatic rings). The vector $\mathbf{r}_{\text{FH}}$ is the director for the dipole–dipole interaction between the fluorine and proton I. The small coordinate frame on the lower right represents the principal axes of the ^{19}F CSA tensor as described in the text.

Overall molecular tumbling and internal motions modulate the orientations of the DD and CSA interaction tensors relative to the external field, $\mathbf{B_0}$. In turn, these orientational fluctuations establish local fluctuating fields that stimulate the transverse and longitudinal relaxation of the fluorine spins. Because the principal axes of the DD and CSA tensors transform identically under rotations, their orientational fluctuations are correlated. This DD-CSA cross-correlation manifests as differential relaxation rates for the fluorine quartet members. Specifically, quartet members associated with proton I spin up will have relaxation rates different than those with proton I spin down. In what follows, we denote spin up and spin down states for the I proton with the superscripts "+" and "−", respectively. $R_2^{\pm}$ and $R_1^{\pm}$ then indicate fluorine transverse and longitudinal relaxation rate constants associated with the two I proton spin states. The two transverse rate constants may then be written as

$$R_2^{\pm} = \Gamma_{\text{TR}} \pm \eta_{xy}, \qquad [1]$$

where

$$\Gamma_{\text{TR}} = R_2^{\text{CSA}} + \frac{1}{2}\left(R_2^{\text{DD}} + R_{2z}^{\text{DD}}\right) + R_{\text{ex}} + \rho_{\text{I}}. \qquad [2]$$

The corresponding expressions for the longitudinal rate constants are

$$R_1^{\pm} = \Gamma_{\text{L}} \pm \eta_z, \qquad [3]$$

where

$$\Gamma_{\text{L}} = R_1^{\text{CSA}} + \frac{1}{2}\left(R_1^{\text{DD}} + R_{zz}^{\text{DD}}\right) + \rho_{\text{I}}. \qquad [4]$$

Equations [1] and [3] show that the relaxation rate constants for the spin up and spin down populations of proton I are the sum of contributions from the individual relaxation mechanisms (the auto-correlation terms), plus interference effects between these mechanisms (the cross-correlation terms). The Γ_{TR} and Γ_{L} terms contain the auto-correlation terms. They include the familiar CSA and DD contributions to the longitudinal and transverse rate constants R_1 and R_2, as well as to R_{zz} and R_{2z}, which describe the relaxation of two-spin orders $2I_zF_z$ and $2I_zF_{xy}$. The ρ_{I} term accounts for longitudinal dipolar relaxation of the *ortho* proton I by other nearby protons. The R_{ex} term allows for the possibility of transverse relaxation enhancements arising from time-dependent modulations in the ^{19}F chemical shift induced by chemical exchange. Here, we restrict our analysis to the "fast"-exchange regime in which only a single fluorine multiplet is observed. In this case, the nonexchange relaxation terms (i.e., $R_{1,2}$, ρ_{I}, and $\eta_{xy,z}$) are understood to be *population-weighted averages* of rate constants belonging to the individual states coupled via chemical exchange.

The transverse and longitudinal cross-correlation terms are η_{xy} and η_z. Their contributions to the rate constants are of opposite sense for the spin up (+) and spin down (−) populations of proton I; hence, they are the source of the differential relaxation. In a basis of Cartesian product operators, this differential relaxation manifests as cross-relaxation between fluorine in-phase coherence ($F_{x,y}$) and antiphase ^{19}F coherence ($2I_zF_{x,y}$), as well as between fluorine Zeeman order (F_z) and longitudinal two-spin order ($2I_zF_z$). The interference terms η_{xy} and η_z are then the rate constants mediating these cross-relaxation pathways.

To study the dynamic information of the cross-correlation rate constants η_{xy} and η_z, we appeal to their formulations in terms of power spectral density functions, which are (*17*)

$$\eta_{xy} = c_x d_{\mathrm{FH}}\left[\frac{2}{3}J_x^{\mathrm{CD}}(0) + \frac{1}{2}J_x^{\mathrm{CD}}(\omega_{\mathrm{F}})\right] + c_y d_{\mathrm{FH}}\left[\frac{2}{3}J_y^{\mathrm{CD}}(0) + \frac{1}{2}J_y^{\mathrm{CD}}(\omega_{\mathrm{F}})\right] \quad [5]$$

$$\eta_z = c_x d_{\mathrm{FH}} J_x^{\mathrm{CD}}(\omega_{\mathrm{F}}) + c_y d_{\mathrm{FH}} J_y^{\mathrm{CD}}(\omega_{\mathrm{F}}). \quad [6]$$

The coefficients $c_u\,(u = x, y)$ and d_{FH} are the CSA and DD interaction strengths, and are aggregates of various physical constants:

$$c_u = \gamma_{\mathrm{F}} B_0(\sigma_{uu} - \sigma_{zz}) \quad [7]$$

$$d_{\mathrm{FH}} = \frac{\gamma_{\mathrm{H}}\gamma_{\mathrm{F}}\hbar}{r_{\mathrm{FH}}^3}. \quad [8]$$

Both the proton and fluorine gyromagnetic ratios are positive with $\gamma_{\mathrm{F}}/\gamma_{\mathrm{H}} \approx 0.94$. The distance between the fluorine and proton I is $r_{\mathrm{FH}} = 2.6$ Å. In Eq. [7], σ_{uu} and σ_{zz} indicate the CSA principal values along the **u** (**u** = **x** or **y**) and **z** axes of the CSA tensor, respectively. The $J_u^{\mathrm{CD}}(\omega)$ functions are cross-correlation power spectral density functions that give the frequency spectrum for the correlated fluctuations between the DD interaction vector $\mathbf{r}_{\mathrm{FH}}$ and the **u**th axis of the CSA tensor. The use of axis-specific spectral densities is consistent with an asymmetric CSA tensor for the aromatic fluorine. Solid state measurements on a fluoro-phenyl ring by Hiyama *et al. (23)* have revealed principal axis values of −75, 0, and 50 ppm, with the most shielded axis (+50 ppm) normal to the plane of the aromatic ring and the least-shielded axis (−75 ppm) lying in the plane of the ring and perpendicular to the CF bond vector. Here, we use the fluoro-phenyl CSA data as a reasonable model for the ^{19}F CSA properties of the aromatic moiety sketched in Fig. 1. Following the conventions of Luck *et al. (9)* we assign the **z**, **y**, and **x** principal axes of the CSA tensor with corresponding principal values of $\sigma_{zz} = -75$ ppm, $\sigma_{yy} = 0$ ppm, and $\sigma_{xx} = 50$ ppm. Figure 1 depicts the orientations of the CSA principal axes relative to the DD interaction vector $\mathbf{r}_{\mathrm{FH}}$. The **x** principal axis makes an angle of 90° with $\mathbf{r}_{\mathrm{FH}}$ and points out of the page. The **y** principal axis makes an angle of 120° with $\mathbf{r}_{\mathrm{FH}}$ and is collinear with the CF bond.

User-specific models of molecular motion give the spectral density functions analytical forms of varying complexity. Here, we adopt a highly simplified form of the Lipari–Szabo spectral density function that assumes isotropic overall tumbling of the fluorinated molecule (*24*). Additionally, the internal flexibility of $\mathbf{r}_{\mathrm{FH}}$ is assumed to consist of small-amplitude angular excursions within the molecule-fixed frame. The cross-correlation spectral density functions then become

$$J_u^{\mathrm{CD}}(\omega) = P_2(\mathbf{u}\cdot\mathbf{n}_{\mathrm{FH}})J^{\mathrm{DD}}(\omega), \quad [9a]$$

where $J^{\mathrm{DD}}(\omega)$ is given by the scaled Lorentzian distribution

$$J^{\mathrm{DD}}(\omega) = \frac{2}{5}\frac{S^2\tau_{\mathrm{c}}}{1+(\omega\tau_{\mathrm{c}})^2}. \quad [9b]$$

$J^{\mathrm{DD}}(\omega)$ is the auto-correlation spectral density function pertaining to the DD relaxation contributions and represents the frequency spectrum for the orientational fluctuations of $\mathbf{r}_{\mathrm{FH}}$ relative to the external magnetic field. $P_2(x)$ is the second-order Legendre polynomial $0.5(3x^2-1)$, $\mathbf{n}_{\mathrm{FH}}$ is a unit vector that lies along $\mathbf{r}_{\mathrm{FH}}$, and **u** is a unit vector along the *u*th principal axis of the CSA tensor. S^2 is the well known generalized order parameter that describes the extent of spatial restriction of the $\mathbf{r}_{\mathrm{FH}}$ internuclear vector (*24*). Internal motion that is completely unrestricted corresponds to $S^2 = 0.0$ while the complete absence of internal motion corresponds to $S^2 = 1.0$. The time scale for the overall isotropic tumbling is set by the correlation time τ_{c}. Consideration of the CSA and DD parameters and the Legendre polynomial in Eq. [9a] reveals that the upfield components of the fluorine multiplet relax more quickly than the downfield components.

The spectral density of Eq. [9a] allows us to consider the variation of η_{xy} and η_z with increasing molecular size, or, equivalently, longer τ_{c}. Figures 2A and 2B simulate this variation for several B_0 field strengths, including 2.4, 7.0, 11.7, and 18.8 T corresponding to proton resonance frequencies of ≈100, 300, 500, and 800 MHz, respectively. The figure assumes the model fluoro-phenyl CSA parameters mentioned above and $S^2 = 0.85$, which is the consensus value derived from protein NMR studies (*25*). The transverse rate constant η_{xy} has a nearly linear dependence on τ_{c} as a consequence of the secular $J_u^{\mathrm{CD}}(0)$ term in Eq. [5]. This implies a more efficient $F_{x,y} \leftrightarrow 2I_zF_{x,y}$ cross-relaxation for larger molecules. In contrast, η_z has only a $J_u^{\mathrm{CD}}(\omega_{\mathrm{F}})$ dependence. As a result, it has a much smaller magnitude than η_{xy}, and peaks at $\tau_{\mathrm{c}} \approx 1/\omega_{\mathrm{F}}$. Such τ_{c} values are associated with high-frequency motions that are characteristic of a rapidly tumbling small molecule ($M_{\mathrm{r}} \leq 500$), or a highly flexible ^{19}F fragment that is bound to a large macromolecule. Figures 2A and 2B also illustrate the variation of η_{xy} and η_z with respect to the field strength B_{o}. Both rate constants have a direct dependence on B_{o} via the CSA coefficients given in Eq. [7],

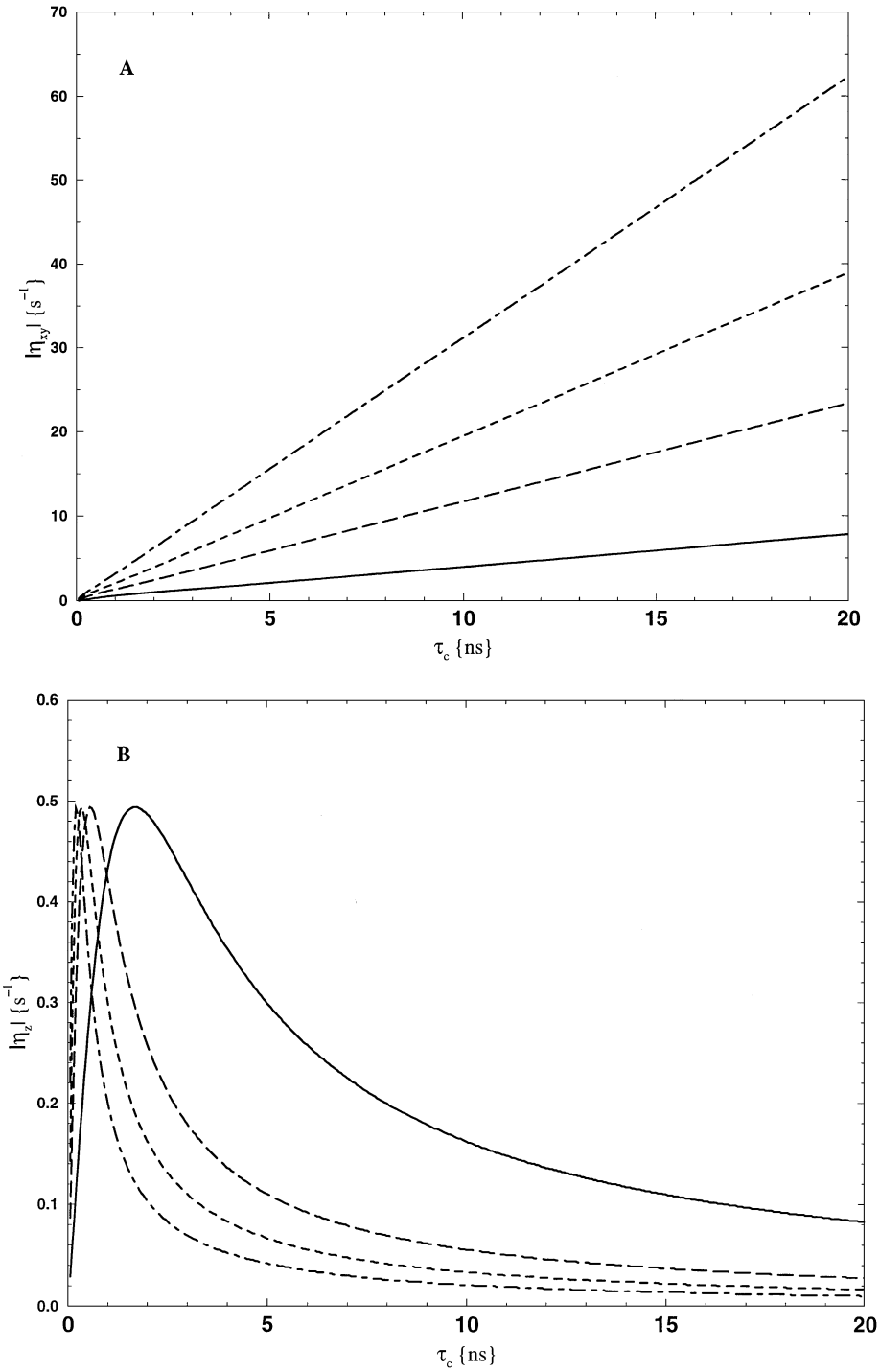

FIG. 2. Variations of fluorine CSA-DD cross-correlation rate constants (A) η_{xy} and (B) η_z with rotational correlation time τ_c and field strength B_o. The plots assume isotropic tumbling of the fluorine moiety and the model CSA parameters of Hiyama *et al*. (*23*). Different magnetic field strengths B_o include 2.4 T (solid line), 7.0 T (long dashed line), 11.7 T (short dashed line), and 18.8 T (dashed–dotted line).

and an indirect dependence via the spectral density functions. Increasing B_o decreases the contribution of all nonsecular samplings of the spectral density functions; thus, large B_o increases η_{xy} but not η_z.

(ii) Transverse cross-correlation measurements as an aid for characterizing exchange processes. Reversible ligand-binding events constitute exchange processes operating on the micro- to millisecond time scale. The transverse auto-relaxation rate

constant $R_2 = 1/T_2$ is sensitive to such processes, as well as the faster pico to nanosecond orientational fluctuations responsible for the CSA and DD relaxation. For NMR studies of binding, one therefore needs to be able to identify and quantify the exchange contributions to R_2. To address this need, one can measure the magnitude ratio $|\eta_{xy}/R_2|$. Protein ^{15}N relaxation studies by Brutscher *et al.* and Fushman and Cowburn have demonstrated the high sensitivity of this ratio to the presence of micro- to millisecond dynamic processes of the protein backbone (*26, 27*).

The high sensitivity of $|\eta_{xy}/R_2|$ to these "slow" dynamic processes arises from the divergent responses of η_{xy} and R_2 to chemical exchange versus fluctuations in molecular orientation. For a discussion of these responses, we consider a small fluorinated ligand that binds reversibly to a large protein target, and is in fast exchange between the free and bound states. The fast-exchange scenario is appealing not only for its simplicity, but also for its congruence with typical experimental conditions in current NMR screening protocols (*28*). We consider first the effects of chemical exchange, and then those of orientational fluctuations.

Fast exchange leads to an averaged R_2 for the exchanging ligand given by (*4*)

$$R_{2,\text{avg}} = P_\text{B} R_{2,\text{B}} + (1 - P_\text{B}) R_{2,\text{F}} + R_\text{ex}. \qquad [10]$$

In Eq. [10], P_B and $(1 - P_\text{B})$ are the equilibrium fractional populations of bound and free ligands, respectively. $R_{2,\text{B}}$ and $R_{2,\text{F}}$ are bound and free state R_2 values. The additional chemical exchange term R_ex is the same as in Eq. [2]. For a simple two-state binding equilibrium, R_ex is given by

$$R_\text{ex} = 4\pi^2 P_\text{B}(1 - P_\text{B})(\delta_\text{F} - \delta_\text{B})^2/k_\text{ex}. \qquad [11]$$

R_ex depends quadratically on the difference in chemical shifts between the free and bound states $(\delta_\text{B} - \delta_\text{F})$, the bound ligand fraction P_B, and the exchange rate constant k_ex. Therefore, R_ex can vanish if the chemical shifts are degenerate, if the populations are skewed, or if k_ex is too fast. For proton NMR in typical screening protocols, one of these conditions is often met. In contrast, fluorine has a much broader chemical shift span (≈900 ppm, (*2*)) and therefore substantial R_ex contributions are more likely. Unlike R_2, η_{xy} is unaffected by R_ex. This is implied in Eqs. [1] and [2], in which R_ex effects equally the I^+ and I^- components of the ^{19}F multiplet. Since η_{xy} is proportional to the difference of R_2^+ and R_2^-, it remains free from R_ex effects. Exchange therefore leads to a simple population-weighted averaging of the free and bound η_{xy} rate constants:

$$\eta_{xy,\text{avg}} = P_\text{B}\eta_{xy,\text{B}} + (1 - P_\text{B})\eta_{xy,\text{F}}. \qquad [12]$$

To appreciate the effects of orientational fluctuations, we temporarily forget R_ex, and consider only the R_2 and η_{xy} rate constants for the free and bound states. Both η_{xy} and R_2 have similar responses to orientational fluctuations, as is evident from their expressions in terms of spectral density functions. The expression for η_{xy} has been given in Eq. [5]. The corresponding expression for R_2 is

$$\begin{aligned} R_2 = {} & \frac{d_\text{FH}}{2} J^\text{DD}(0) + \frac{1}{9}\left\{c_x^2 J_x^\text{CSA}(0) + c_y^2 J_y^\text{CSA}(0)\right. \\ & \left. + 2c_x c_y J_x^\text{CSA}(0)\right\} + \frac{3d_\text{FH}}{8} J^\text{DD}(\omega_F) \\ & + \frac{1}{6}\left\{c_x^2 J_x^\text{CSA}(\omega_\text{F}) + c_y^2 J_y^\text{CSA}(\omega_F) + 2c_x c_y J_{xy}^\text{CSA}(\omega_\text{F})\right\} \\ & + \frac{d_\text{FH}}{8}\left\{J^\text{DD}(\omega_H - \omega_F) + 6J^\text{DD}(\omega_\text{H}) + 6J^\text{DD}(\omega_\text{H} + \omega_\text{F})\right\}. \end{aligned} \qquad [13]$$

The similarity between η_{xy} and R_2 becomes most apparent if we use the isotropic spectral density function shown in Eqs. [9a] and [9b]. Then we are faced with just one unique spectral density function since $J_x^\text{CSA}(\omega) = J_y^\text{CSA}(\omega) = 0.5J_{xy}^\text{CSA}(\omega) = J^\text{DD}(\omega)$, and $J_u^\text{CD}(\omega) = P_2(\mathbf{u}\cdot\mathbf{n}_\text{FH})J^\text{DD}(\omega)$. The result is a nearly identical dependence for η_{xy} and R_2 on the CSA/DD spectral density functions evaluated at 0 and ω_F. The chief differences are the higher-frequency spectral densities $J^\text{DD}(\omega_\text{H})$, $J^\text{DD}(\omega_\text{H} \pm \omega_\text{F})$ that are present in R_2 (terms proportional to $d_\text{FH}/8$ in Eq. [13]) but absent in η_{xy}. If we can neglect these higher-frequency terms, then the spectral density dependence factors out of the $|\eta_{xy}/R_2|$ ratio, which then becomes independent from overall rotational diffusion (*26, 27*).

The higher-frequency spectral densities may be negligible for two reasons. For example, for large molecules, $J^\text{DD}(0) \gg J^\text{DD}(\omega_\text{H} \pm \omega_\text{F})$ and the latter can therefore be ignored, or the DD contributions may be inherently smaller than those of the CSA contributions. A comparison of the CSA interaction strengths c_x^2 and c_y^2 with the DD strength d_FH^2 in Eqs. [7] and [8] can query this possibility. Using the model CSA parameters, a field strength of 11.7 T, and an internuclear distance of $r_\text{FH} = 2.6$ Å, we find that $|d_\text{FH}/c_x|^2 \approx 0.08$ and $|d_\text{FH}/c_y|^2 \approx 0.04$. These small ratios demonstrate that transverse relaxation of the aromatic fluorine at 11.7 T is dominated by the CSA mechanism; this suggests that the high-frequency spectral densities $J^\text{DD}(\omega_\text{H})$, $J^\text{DD}(\omega_\text{H} \pm \omega_\text{F})$ of the ^{19}F–^{1}H DD interaction may be neglected in the $|\eta_{xy}/R_2|$ ratio over a wide range of correlation times τ_c.

Figure 3 plots the $|\eta_{xy}/R_2|$ ratio as a function of overall correlation time τ_c for several magnetic field strengths. Two features are worth nothing. First, the ratio increases with τ_c and reaches a plateau value above some critical value. This critical τ_c value decreases at higher field strength B_o on account of the increasing dominance of the CSA relaxation mechanism. Second, the breadth of $|\eta_{xy}/R_2|$ values becomes increasingly narrow at higher B_o. For example, at 11.7 T, the ratio is expected to increase only by about 6% as τ_c increases from 50 ps to 50 ns. Thus, if we consider the effects of molecular tumbling

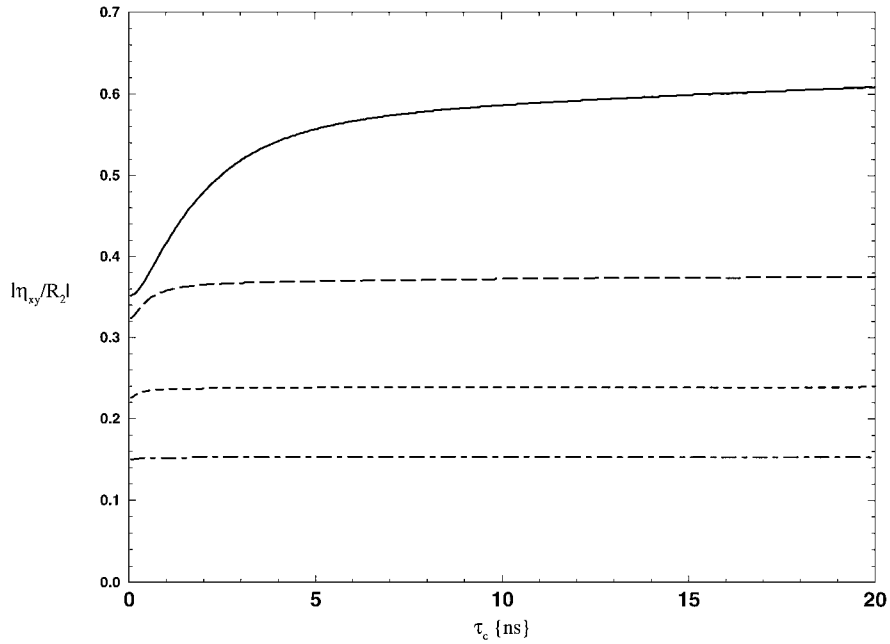

FIG. 3. Variation of the magnitude ratio $|\eta_{xy}/R_2|$ in the absence of exchange broadening terms R_{ex} with rotational correlation time τ_c and field strength B_o. The plot assumes rigid isotropic tumbling and field strengths including 2.4 T (solid line), 7.0 T (long dashed line), 11.7 T (short dashed line), and 18.8 T (dashed–dotted line). At higher field, the ratio becomes almost independent of τ_c over the entire range of correlation times.

alone, we anticipate little change in the $|\eta_{xy}/R_2|$ ratio for a ^{19}F ligand that goes from a state of free tumbling, to one in which it is bound to a high molecular weight receptor. Accordingly, we expect $|\eta_{xy,F}/R_{2,F}| \approx |\eta_{xy,B}/R_{2,B}|$. In turn, this near equality implies that the exchange-averaged ratio will also be essentially unchanged from the free state value.

The dominance of the CSA relaxation mechanism for the aromatic fluorine therefore allows the definition of a characteristic ratio, $|\eta_{xy}/R_2|$, that is practically independent of the rapid pico- to nanosecond motions associated with orientational fluctuations. Increases in molecular weight cause only minor or negligible *increases* in $|\eta_{xy}/R_2|$. Exchange processes lead to averaged rate constants, $\eta_{xy,avg}$ and $R_{2,avg}$. Accordingly, we expect that the ratio of the averaged rate constants, $|\eta_{xy,avg}/R_{2,avg}|$, to be almost unchanged from those measured in the separate states, provided $R_{ex} \approx 0$. If, however, the chemical exchange does entail a significant R_{ex}, then $R_{2,avg}$ will be increased by R_{ex} but $\eta_{xy,avg}$ will not. The ratio $|\eta_{xy,avg}/R_{2,avg}|$ will then show an "anomalous" decrease. Comparisons of this ratio for fluorine moieties in different microenvironments therefore provide a means for identifying, localizing, and comparing exchange processes. This feature is of special interest for molecular recognition studies since the dynamics mediating recognition typically operate on these "slower" time scales.

(iii) Cross-correlation measurements as a means for improving the accuracy of binding affinity estimates by NMR relaxation. Once a R_{ex} contribution has been identified, various follow-up strategies may be used to probe for the underlying exchange rate constants. One strategy measures $R_{1\rho}$, which is the relaxation rate constant for magnetization along an effective field in the rotating frame. More specifically, one observes the dependence of $R_{1\rho}$ on the effective field magnitude (*4*). This dependence, or dispersion, is then fitted to an analytical function that includes the exchange rate constant as one of the fitting parameters. As with rotational fluctuations, the form of the analytical function depends on the model used to describe the exchange process. Here, the fluorine effective field is achieved using a continuous-wave (CW) radiofrequency spin lock with an (rf) field of magnitude $\gamma_F B_{rf}$. The spin lock is applied on resonance with the exchange-averaged fluorine chemical shift, $\delta_{avg} = P_B\delta_B + (1 - P_B)\delta_F$. If we assume the same two-state exchange as above, and that $\gamma_F B_{rf} > |\delta_F - \delta_B|$, then $R_{1\rho}$ gains a functional dependence on $\gamma_F B_{rf}$ given by (*3, 4, 29*)

$$R_{1\rho}(\gamma_F B_{rf}) = R_2^{NE} + \frac{A/k_{ex}}{1 + (\gamma_F B_{rf}/k_{ex})^2}. \qquad [14]$$

Equation [14] describes a Lorentzian of half-width k_{ex} squatting on a plateau value of R_2^{NE}. The desired exchange rate constant is k_{ex}, which is related to the bound ligand fraction P_B and the ligand off-rate via the ratio $k_{ex} = k_{off}/(1 - P_B)$. Under a large ligand excess typical of screening protocols, $P_B \ll 1$ and therefore k_{ex} well approximates k_{off}. The amplitude factor A is related to R_{ex} (cf. Eq. [11]) via the product $A = R_{ex}k_{ex}$. From the Lorentzian form of Eq. [14], we expect that $R_{1\rho}$ decreases as $\gamma_F B_{rf}$ increases. In the limit that $\gamma_F B_{rf} \gg k_{ex}$, one approaches

R_2^{NE} asymptotically. Note that R_2^{NE} contains only the nonexchange contributions to $R_{1\rho}$ that stem from the CSA and DD relaxation mechanisms. Under the reasonable assumption that the CSA and DD spectral densities satisfy $J(\omega \pm \gamma_F B_{rf}) \approx J(\omega)$, R_2^{NE} is then given by the $R_{2,avg}$ in Eq. [10] minus the R_{ex} term:

$$R_2^{NE} = P_B R_{2,B} + (1 - P_B) R_{2,F}. \quad [15]$$

Note that the informative dependence of $R_{1\rho}$ on $\gamma_F B_{rf}$ can escape detection if there is a severe mismatch between k_{ex} and $\gamma_F B_{rf}$, or if R_{ex} becomes too small.

To determine the desired exchange rate constant k_{ex}, one fits the $\gamma_F B_{rf}$ dependence of $R_{1\rho}$ to Eq. [14], using A, R_2^{NE}, and k_{ex} as the three adjustable parameters. However, accurate fits of k_{ex} are practically impossible unless the experimental $R_{1\rho}$ values sample the full range of Eq. [14]. In particular, it is crucial to have data that samples the *non*exchange contributions to $R_{1\rho}$ (i.e., the plateau value R_2^{NE}) since the fitted k_{ex} value is extremely sensitive to that of R_2^{NE}. In principal, R_2^{NE} can be extracted directly from the $R_{1\rho}$ data, provided $\gamma_F B_{rf}$ can be made sufficiently strong to satisfy $\gamma_F B_{rf} \gg k_{ex}$. In practice, such strong rf-field strengths are often impossible due to considerations of sample integrity or hardware limitations. Moreover, the weakly binding ligands detected by NMR screening can have k_{ex} values that exceed the acceptable range of rf-field strengths. We therefore need an alternate means of estimating R_2^{NE} that does not rely on $R_{1\rho}$. Measurements of the $|\eta_{xy}/R_2|$ ratio can provide this means. Specifically, we can first measure $|\eta_{xy,F}/R_{2,F}|$ for the free ligand. Assuming an absence of exchange broadening in the free state, this ratio reflects only the CSA and DD relaxation. Under the aforementioned caveats, we then exploit the insensitivity of this ratio to changes in rotational correlation time, and assert that this ratio is maintained in the bound state, i.e., $|\eta_{xy,B}/R_{2,B}| \approx |\eta_{xy,F}/R_{2,F}|$. Substitution of this relation into the fast-exchange expressions of Eqs. [12] and [15] then yields $|\eta_{xy,F}/R_{2,F}| \approx |\eta_{xy,avg}/R_2^{NE}|$. This last relation then allows one to estimate R_2^{NE} independently from $R_{1\rho}$ through measurements of the free state $\eta_{xy,F}$ and $R_{2,F}$, and the exchange-averaged $\eta_{xy,avg}$. The transverse cross-correlation measurements therefore enable the estimation of the nonexchange contribution to $R_{1\rho}$, which is crucial for the accurate estimations of the k_{ex} exchange rate constants. As such, the $|\eta_{xy}/R_{2,F}|$ ratio can be a powerful aid for accurate analysis of $R_{1\rho}$ measurements aimed at rank-ordering binding affinities.

III. PULSE SCHEMES AND RESULTS

As discussed above, the transverse cross-correlation rate constant η_{xy} is more sensitive than η_z to changes in overall molecular tumbling. Additionally, it can help pinpoint exchange processes. Thus, from the standpoint of ligand–receptor interactions η_{xy} is of greater interest, and we present below three pulse schemes that focus on its exploitation. The first two sequences use the CSA-DD cross correlation as a means for generating ^{19}F–^{1}H correlation spectra. The third scheme measures η_{xy} for subsequent use in ligand-binding experiments.

(i) ^{1}H detected cross-correlation. The simple pulse scheme of Fig. 4A provides evidence of the transverse ^{19}F–^{1}H CSA-DD

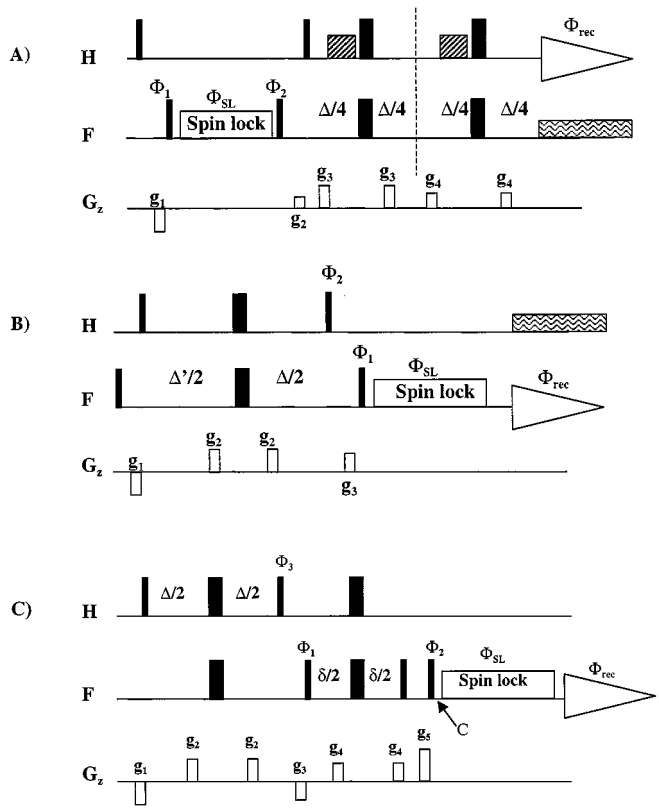

FIG. 4. ^{19}F–^{1}H pulse schemes for detecting and quantifying transverse cross-correlation effects. Thin and thick vertical bars indicate 90° and 180° pulses, respectively. Pulses without explicit phase symbols are along $+x$. (A) Fluorine to proton transfer via transverse cross-correlated cross-relaxation. Phase cycling is as follows: $\phi_1 = +y, -y, \phi_2 = 2(+y), 2(-y), \phi_{sl} = x$, and $\phi_{rec} = +x, -x, -x, +x$. The low shaded pulses are low-powered 2-ms rectangular 180° pulses of phase opposite from that of the adjacent hard 180° pulses. The proton signal is recorded with fluorine decoupling. Rectangular gradients are applied along the z axis with the following durations and strengths: $g_1 = 1$ ms, −12.5 G/cm; $g_2 = 1$ ms, 13.7 G/cm; $g_3 = 800$ μs, 20 G/cm; $g_4 = 800$ μs, 15.3 G/cm. (B) Proton to fluorine transfer via transverse cross-correlated cross-relaxation. Phase cycling is as follows: $\phi_1 = 4(+y)$, $4(-y)$, $\phi_2 = 2(+y)$, $2(-y)$, $\phi_{sl} = +x, -x$, and $\phi_{rec} = 2(+x)$, $4(-x)$, $2(+x)$. The signal is detected with proton decoupling. Rectangular gradients are applied along the z axis with the following durations and strengths $g_1 = 1$ ms, −13 G/cm; $g_2 = 800$ μs, 9.5 G/cm; $g_3 = 1$ ms 14.3 G/cm. (C) Measurement of η_{xy}. Phase cycling is as follows: $\phi_1 = +y$, $-y$, $\phi_2 = 4(+y)$, $4(-y)$, $4(-x)$, $4(+x)$, $\phi_{sl} = 2(+x)$, $4(-x)$, $2(+x)$, $2(+y)$, $4(-y)$, $2(+y)$, and $\phi_{rec} = 2(-y, +y)$, $2(+y, -y)$, $2(+x, -x)$, $2(-x, +x)$. For downfield selection, $\phi_3 = -y$ and for upfield selection $\phi_3 = +y$. Delays are $\Delta = 23$ ms and $\delta = 19$ ms. The delay δ was varied until optimal suppression of the unwanted doublet member was achieved. Gradients were rectangular pulses with the following durations and strengths: $g_1 = 500$ μs, 7 G/cm; $g_2 = 1$ ms, 20.1 G/cm; $g_3 = 500$ μs, 12.4 G/cm; $g_4 = 1$ ms, 14.9 G/cm. For all experiments, a simple CW long pulse of length T_{lock} and strength $\gamma_F B_1 \approx 2$ kHz was used for spin locking.

cross-correlation. In brief, the scheme generates proton coherence from the ^{19}F magnetization by way of the CSA-DD cross-relaxation pathway $F_{x,y} \leftrightarrow 2I_zF_{x,y}$. The initial proton 90° is followed by a purge gradient to ensure that no signal originates from the proton equilibrium magnetization. A ^{19}F 90 pulse then places the ^{19}F magnetization alternately on the $\pm x$ axis. Subsequent spin locking along the x axis suppresses chemical shift and scalar coupling evolution while encouraging the cross-correlated cross-relaxation. Just after the spin lock, we have an admixture of F_x and $2I_zF_x$. Application of the last pair of 90° pulses transfers fluorine $2I_zF_x$ coherence to proton $2F_zI_y$ coherence. The concluding two spin echoes refocus the antiphase $2F_zI_y$ to I_x via INEPT (*30*), while simultaneously suppressing water via the excitation sculpting method of Hwang and Shaka (*31*). The total INEPT refocusing time is Δ. Due to the small proton–fluorine scalar coupling constants (8–12 Hz), rather long delays Δ are necessary and proton–proton scalar coupling evolution causes some defocusing. The proton signal is read out with ^{19}F decoupling. Longitudinal cross-correlation is detected by the analogous pulse sequence in which the spin lock is replaced by a simple relaxation delay, and the first ^{19}F 90° is replaced by 90°_x(F)–$90^\circ_{\pm x}$(F). Application of this sequence to the compound containing the molecular fragment of Fig. 1 yields a single peak at 7.07 ppm corresponding to proton I (data not shown).

(ii) ^{19}F detected cross-correlation. Figure 4B shows an alternative method using fluorine observation. Initially, a 90°_x(F)–gradient combination ensures that the observed signal stems only from proton magnetization. An INEPT spin-echo period then creates proton coherence that becomes antiphase with respect to the fluorine and other scalar coupled protons. As before, the INEPT delay uses $\Delta' = \Delta = 1/4J_{\mathrm{IF}} \approx 21$ ms. This fixed delay period can be converted into a constant-time proton chemical shift evolution period, thereby converting the sequence into a two-dimensional (2D) ^{19}F–^{1}H correlation experiment driven by cross-correlated transfer. In this case Δ' becomes $1/4J_{\mathrm{IF}} - t_1/2$ and Δ becomes $1/4J_{\mathrm{IF}} + t_1/2$. Before the second proton 90°(H), we have an admixture of I_y and $2I_xF_z$. The subsequent pair of 90° pulses converts antiphase $2I_xF_z$ to $2I_zF_x$. Spin locking of the antiphase coherence leads to the growth of in-phase F_x via cross-correlated cross-relaxation. The latter operator is detected in the presence of proton decoupling. An example of the 2D version of this experiment is shown in Fig. 5 for the fluorinated aromatic compound of Fig. 1. This molecule gives only a single cross peak since we have only one significant ^{19}F–^{1}H dipolar interaction. In the more general case, we may have multiple ^{19}F–^{1}H dipolar interactions leading to multiple CSA-DD cross-relaxation pathways. In these cases, the 2D spectrum is advantageous in that the various cross-correlations can be resolved via the proton chemical shift.

(iii) Pulse scheme for measurements of η_{xy} via transverse relaxation measurements of individual multiplet components. For ligand dynamics studies, we need methods for quantifying η_{xy} in order to estimate the $|\eta_{xy}/R_2|$ ratio. We accomplish this using a fluorine-detection approach in which one simply

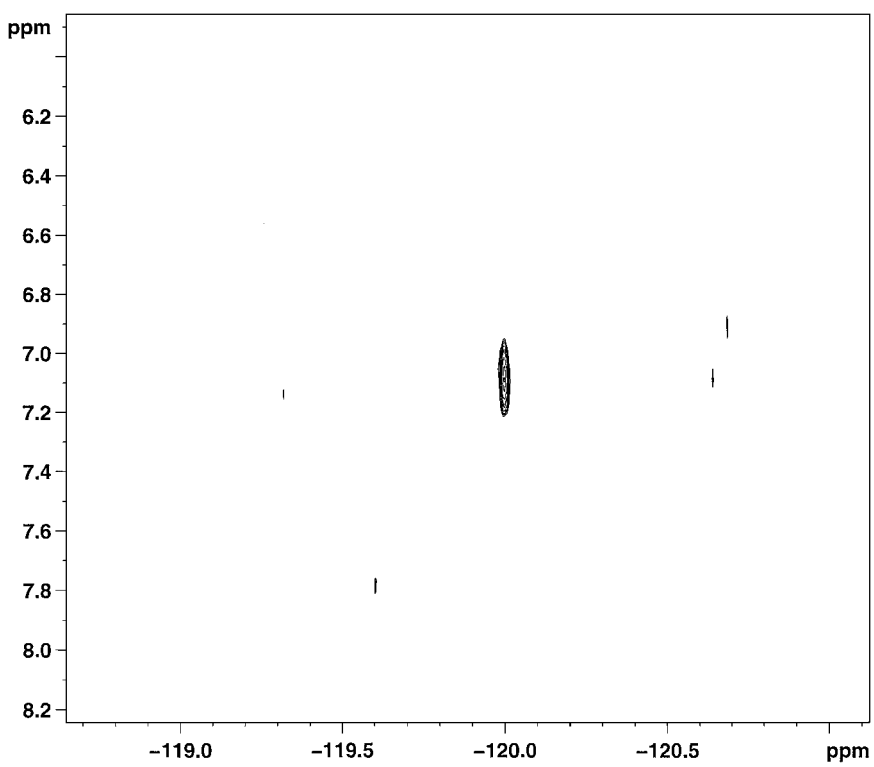

FIG. 5. An example of 2D ^{19}F–^{1}H correlation spectra using cross-correlated cross-relaxation and the pulse scheme of Fig. 4B.

measures the relaxation rates for the individual multiplet components. To enhance the accuracy of these measurements, we use a sequence that edits for specific members of the fluorine quartet by creating an appropriate admixture of the equilibrium ^{19}F and ^{1}H magnetizations. The sequence is shown in Fig. 4C. The approach is based on the TROSY methods for aromatic ^{13}C–^{1}H correlation spectra proposed by Pervushin *et al*. (*32*). Note that since $|\gamma_F/\gamma_H|^2 = 0.88$, the ^{19}F and ^{1}H equilibrium magnetizations are comparable. The sequence begins with an initial INEPT period to create proton coherence that is antiphase with respect to the fluorine. Simultaneously, the INEPT block merely inverts the fluorine equilibrium magnetization. After the second proton 90°, a gradient z-filter selects for longitudinal fluorine magnetization that includes both the two-spin orders $2I_zF_z$, $2S_zF_z$, originating from the ^{1}H equilibrium magnetization, as well as simple Zeeman (one-spin) fluorine magnetization. A $90^\circ_{\pm y}$(F) pulse then transforms these operators into a superposition of four transverse magnetizations along the $\pm x$ axis, where each magnetization corresponds to a particular member of the fluorine quartet. The transverse magnetizations corresponding to the outer and inner quartet lines evolve with effective coupling constants that are the sum and difference of the J_{IF} and J_{SF} coupling constants, respectively. After a total evolution time of $\delta \approx 1/2(J_{IF} + J_{SF})$, the outer quartet member magnetizations are along the $\pm y$ axis while the inner lines have rotated only marginally away from the $\pm x$ axis. A 90°_x(F) pulse then stores the majority of the outer lines on the $\pm z$ axis while leaving the inner lines nearly unaffected. A gradient pulse (g_5) preferentially dephases the inner line magnetizations and the following 90°_y(F) pulse returns the outer line magnetizations to the transverse plane. Their relative magnitudes depend on the value of ϕ_3. A density operator description articulates this dependence. Specifically, the components of the density operator corresponding to these transverse magnetizations can be expressed in terms of projector operators that refer to the specific quartet members (*33*). As before, using "+" for spin up and "−" for spin down, and the identities

$$P^{++} = \frac{1}{4}(E + 2I_z + 2S_z + 4I_zS_z) \qquad [16]$$

$$P^{--} = \frac{1}{4}(E - 2I_z - 2S_z + 4I_zS_z), \qquad [17]$$

the relevant terms of the density operator at point C are

$$\sigma(C) = \sin\alpha\left((-)^n M_H^{eq}\varepsilon(\Delta) - M_F^{eq}\right)P^{++}F_x + \sin\alpha\left((-)^n M_H^{eq}\varepsilon(\Delta) + M_F^{eq}\right)P^{--}F_x, \qquad [18]$$

where

$$\varepsilon(\Delta) = \sin\pi J_{IF}\Delta + \sin\pi J_{SF}\Delta\cos\pi J_{SK}\Delta. \qquad [19]$$

In Eqs. [16] and [17], E, I, and S are the identity, I proton, and S proton operators, respectively. In Eq. [18], the product operators $P^{++}F_x$ and $P^{-}F_x$ refer to x magnetizations for the outer lines of the fluorine quartet. The symbols M_H^{eq} and M_F^{eq} are the equilibrium z magnetizations for proton and fluorine, respectively. The argument of the sine function is $\alpha = \pi(J_{IF} + J_{SF})\delta$. The exponent n is 1 or 2, if ϕ_3 is $+y$ or $-y$, respectively. If $n = 1$, the signals stemming from the proton and fluorine equilibrium magnetizations add for the $P^{++}F_x$ quartet member and subtract for the $P^{-}F_x$ member, thereby selecting for $P^{++}F_x$. Alternatively, the choice of $\phi_3 = -y$ sets $n = 2$, and we enhance $P^{-}F_x$ and attenuate $P^{++}F_x$. We found that a delay of $\Delta \approx 12.5$ ms produced optimal suppression for either scenario. The stacked 1D-fluorine spectra of Fig. 6 illustrate the selection process described. The top and middle traces show the spectra obtained from the pulse sequence of Fig. 4C just prior to the spin lock (point C) with $\phi_3 = -y$ (top) and $+y$ (middle). These traces may be compared to the standard proton-coupled 1D spectrum shown in the bottom trace. Whereas the bottom trace displays the full fluorine quartet, the top and middle traces show selection for only the downfield and upfield quartet members, respectively. Primarily the outer lines are retained ($P^{++}F_x$, $P^{--}F_x$) with lesser contributions from the inner lines ($P^{+-}F_x$, $P^{-+}F_x$).

Having achieved the appropriate quartet member selection, the application of a fluorine spin lock along the x-axis after point C then allows measurement of the associated transverse relaxation rate. The resulting signals are detected without proton decoupling. As noted above, the SF dipolar interaction is negligible compared to the IF interaction. Thus, for CSA-DD cross-correlation effects here, the state of the S spin is irrelevant and the transverse relaxation rate constants for $P^{++}F_x$ and $P^{+-}F_x$ are given by R_2^+ and those for $P^{-+}F_x$ and $P^{--}F_x$ are given by R_2^- (cf. Eq [1]). The magnitude difference of the two rate constants R_2^+ and R_2^- gives an estimate of $2|\eta_{xy}|$.

The above strategy may be compared to the current methods for measuring η_{xy} for ^{15}N–^{1}H spin systems (*18*, *19*). These methods employ multiple INEPT periods of duration $1/2J_{NH}$ to detect separately auto-relaxation of N_x and cross-correlated cross-relaxation between N_x and $2I_zN_x$. These methods are sensitive for ^{15}N–^{1}H spin systems due to the large heteronuclear scalar coupling constant, $J_{NH} \approx 90$ Hz, which allows ample INEPT transfer with minimal transverse relaxation losses. However, for the aromatic ^{19}F–^{1}H spin system, $J_{IF} = 12$ Hz, leading to INEPT periods of ≈42 ms. Such long delays are not well suited for the fluorine work presented here. In particular, the high sensitivity of ^{19}F to exchange broadening exacerbates the transverse relaxation losses during INEPT spin-echo segments. The method described above involves transverse fluorine magnetization for $\approx 1/4J_{FH}$ as opposed to $1/2J_{FH}$, and therefore retains greater sensitivity.

(iv) Observed behavior of $|\eta_{xy}/R_2|$ versus τ_c. To study the behavior of $|\eta_{xy}/R_2|$ as a function of the overall rotational

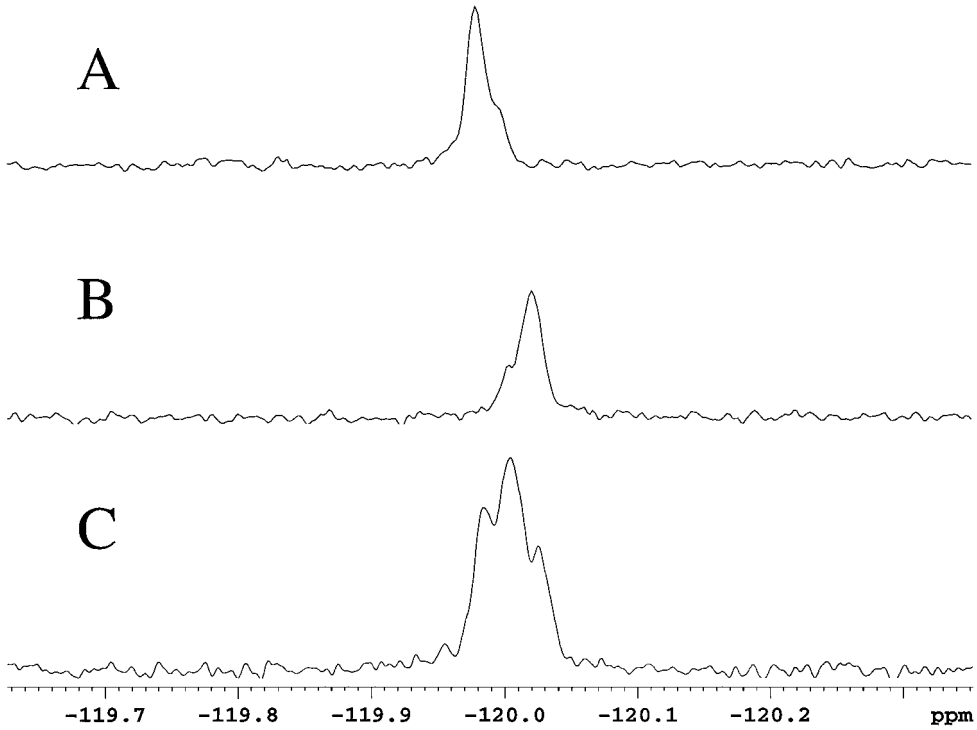

FIG. 6. Example of quartet component selection using the pulse scheme of Fig. 4C. Top and middle traces correspond to the downfield (A) and upfield (B) quartet components selected by setting $\phi_3 = -y$ and $+y$, respectively. For comparison, the bottom-most trace shows the standard proton-coupled fluorine spectrum (C).

correlation time, τ_c, we measured both parameters for a small fluorinated compound ($M_r = 242$) containing the aromatic schematic of Fig. 1 as its core. To access longer correlation times, the compound was dissolved in a buffer containing 50% (v/v) *d*-glycerol. We used the sequence of Fig. 4C to estimate η_{xy}, and a compensated CPMG sequence (*16*, *34*) to measure R_2. We further supplemented these measurements with CW on-resonance ^{19}F $R_{1\rho}$ measurements using rf field strengths of 4335 and 771 Hz. The experiments were recorded at three temperatures including 22, 14, and 10°C, and the results are listed in Table 1.

At all temperatures, only a single fluorine multiplet is observed. The magnitudes of η_{xy} and R_2 both increase with decreasing temperature. This is consistent with longer τ_c values caused by the increased viscosity at lower temperature. Inspection of Table 1 shows that $|\eta_{xy}|$ and R_2 both approximately double when going to 10 from 22°C. However, give the estimated errors, their ratios show no significant changes. To place some bounds on the overall correlation time τ_c, a proton NOESY was run on the same sample at 11.7 T, 10°C, with 100 ms mixing time. The cross peaks are of the same sign as the diagonal, suggesting a τ_c value greater than ≈370 ps/rad. The two ^{19}F $R_{1\rho}$ measurements act as a coarse-grained probe for the presence of exchange dynamics. At all temperatures, the $R_{1\rho}$ values show no significant change from $\gamma_F B_{rf}/2\pi = 770$ to 4330 Hz, thereby suggesting an absence of exchange processes in this frequency range. Taken together, the data suggests that the free molecule conditions are a reasonable approximation of an exchange-free state, and that the $|\eta_{xy}/R_2|$ ratio demonstrates the expected insensitivity to changes in rotational diffusion (τ_c) as simulated by Fig. 3.

(v) Estimation of the binding affinity (K_D) of a small ligand to a protein receptor target using η_{xy} and $R_{1\rho}$. We then

TABLE 1
Magnitudes of Ratios of CSA-DD Transverse Cross-relaxation Rates η_{xy} and the Transverse Auto-relaxation Rate R_2 at 11.7 T

Sample[a]	Temperature (°C)	$\lvert\eta_{xy}\rvert$ (s^{-1})	R_2 (s^{-1})[b]	$\lvert\eta_{xy}/R_2\rvert$[c]
1 mM ligand 50% v/v *d*-glycerol	10	2.91 ± 0.10	10.04 ± 0.04	0.29 ± 0.01
1 mM ligand, 50% v/v *d*-glycerol	14	2.27 ± 0.06	7.92 ± 0.02	0.29 ± 0.01
1 mM ligand, 50% v/v *d*-glycerol	22	1.67 ± 0.06	5.64 ± 0.02	0.30 ± 0.01
1 mM ligand	22	0.36 ± 0.05	1.45 ± 0.02	0.25 ± 0.04
1 mM ligand+ 70 μM receptor	22	1.42 ± 0.08	14.7 ± 0.22	0.10 ± 0.01

[a] Ligand has a molecular weight of 242 Da and contains the singly fluorinated moiety shown in Fig. 1. The receptor is a 15,400-Da protein.

[b] Measured using compensated CPMG sequence.

[c] For the ligand and receptor mixture, the η_{xy} and R_2 are exchange-averaged rate constants.

investigated how the binding interaction between the compound and a known protein receptor influences η_{xy} and R_2. Two 500-μl samples were prepared: one containing a free compound at 1 mM, and another containing a compound at 1 mM in the presence of the protein target at 70 μM. The $|\eta_{xy}/R_2|$ ratios were determined using the same procedures as above, and the results are given in Table 1.

Both samples yield a single ^{19}F quartet, with the protein-containing sample showing a broader linewidth. This suggests that the compound exchanges rapidly between the free and bound states. The exchange toggles the relaxation properties of the fluorine between those of the freely tumbling small molecule (short τ_c), and those of the large protein–ligand complex (long τ_c). Following the Theory section, in the absence of R_{ex} contributions, we expect that the ratio for the exchanging compound to remain unchanged, or increase only slightly from that of the free compound: $|\eta_{xy,avg}/R_{2,avg}| \approx |\eta_{xy,F}|/R_{2,F}|$. Alternatively, if the net R_2 for the exchanging ligand does harbor a R_{ex} term, then the observed ratio for the exchanging ligand should decrease relative to the free compound.

A comparison of the $|\eta_{xy,F}/R_{2,F}|$ and $|\eta_{xy,avg}/R_{2,avg}|$ ratios for the free and exchanging compounds shows that the presence of protein decreases the $|\eta_{xy,avg}/R_{2,avg}|$ ratio to ≈40% of the free compound value. The magnitude of the decrease exceeds the estimated statistical errors, and points to a significant R_{ex} contribution to $R_{2,avg}$. Since the contribution is induced by the presence of protein, its most probable cause is the binding exchange that modulates the fluorine chemical shift.

We would like to determine what fraction of $R_{2,avg}$ can be attributed to R_{ex}. The insensitivity of $|\eta_{xy}/R_2|$ to changes in τ_c provides a means for ascertaining this. Specifically, we can estimate R_2^{NE} (cf. Eq. [11]), which is the nonexchange contribution to $R_{2,avg}$, by exploiting the relation $|\eta_{xy,F}|/R_{2,F}| \approx |\eta_{xy,B}/R_{2,B}|$. The latter equivalence implies that $|\eta_{xy,F}/R_{2,F}| \approx |\eta_{xy,avg}/R_2^{NE}|$, and one can then solve for R_2^{NE}. Using results of Table 1, we estimate that $R_2^{NE} \approx 5.9 \pm 0.9\ s^{-1}$ for the exchanging compound. The residual R_{ex} contribution (which is partially attenuated by the CPMG sequence used) is then given by the difference $R_{ex} \approx R_{2,avg} - R_2^{NE} \approx 8.8 \pm 0.9\ s^{-1}$. Having this estimate enables one to separate the contributions of chemical exchange versus orientational fluctuations to the total fluorine linewidth of the exchanging ligand.

To articulate the exchange rate constants responsible for an observed R_{ex} contribution, one can use rotating frame $R_{1\rho}$ measurements. Recalling Eqs. [14] and [15], in limit that $\gamma_F B_{rf}$ becomes infinitely strong, $R_{1\rho}$ reduces to the nonexchange contribution, R_2^{NE}. Of course, one cannot increase $\gamma_F B_{rf}$ to arbitrarily intense powers lest one risk irreversible damage to the sample or rf coil. Instead, we are limited to some $\gamma_F B_{rf,max}$. Therefore, we expect that $R_{1\rho}$ ($\gamma_F B_{rf,max}$) should be greater than or equal to the R_2^{NE} value estimated via the $|\eta_{xy}/R_2|$ ratios. To verify this, we performed on-resonance CW $R_{1\rho}$ measurements on both the free and exchanging compound at seven spin lock field strengths, including effective field strengths, including $\gamma_F B_{rf}/2\pi \approx 836$, 1181, 1168, 2356, 3328 (x2), and 4701 Hz. The $R_{1\rho}$ values show no dispersion with effective field strength for the free compound. Furthermore, within the estimated errors, the $R_{1\rho}$ values for the free ligand are identical to the CPMG R_2 values. This is consistent with the free ligand sample acting as an exchange-free reference. In contrast, the exchanging ligand shows a clear dispersion, which is illustrated in Fig. 7. After $\gamma_F B_{rf}/2\pi \approx 4700$ Hz, the $R_{1\rho}$ value reaches an apparent plateau value of $6.5 \pm 0.1\ s^{-1}$. The cross-correlation measurements predict an R_2^{NE} value of $5.9 \pm 0.9\ s^{-1}$. Given the estimated errors, these values compare favorably. Their proximity suggests that (i) the use of $|\eta_{xy}/R_2|$ to define R_2^{NE} is reasonable, and that (ii) we are not *missing* significantly greater $R_{1\rho}$ dispersions at higher rf field strengths.

We performed a three-parameter fit of the $R_{1\rho}$ data to Eq. [14]. The three adjustable parameters included R_2^{NE}, the amplitude factor A, and the exchange rate constant, k_{ex}. We used the $|\eta_{xy}/R_2|$ measurements to provide the initial estimate for the R_2^{NE} plateau value. The final fits gave an exchange rate constant of $k_{ex} = 5800 \pm 180\ s^{-1}$.

In our $R_{1\rho}$ dispersion study, we were fortunate that the spin lock field strengths $\gamma_F B_{rf}$ were able to exceed k_{ex}, and thereby define the R_2^{NE} value. However, in general, this need not be true, and it is for these more general situations that the utility of the $|\eta_{xy}/R_2|$ measurements is greatest. More specifically, problems associated with rf heating can restrict the maximal $\gamma_F B_{rf}$ to values substantially less than k_{ex}. In such cases, one cannot define R_2^{NE} experimentally. This lack of definition can compromise the accuracy of the three-parameter fits to Eq. [14], leading to erroneous estimates of k_{ex}. In these situations, measurements of the $|\eta_{xy}/R_2|$ ratio can help improve the accuracy of the fits by providing an independent estimate of R_2^{NE}. In effect, the $|\eta_{xy}/R_2|$ ratio absolves $\gamma_F B_{rf}$ from the sole responsibility of exceeding the *a priori* unknown k_{ex}, and therefore accurate exchange rate constants can still be obtained even if the spin lock field strength is limited.

The exchange rate constant k_{ex} is of keen interest since it approximates k_{off}, which is the unimolecular dissociation rate constant for the ligand–receptor complex. As stated, for the one-step binding equilibrium, $[L] + [E] \leftrightarrow [EL]$, we have $k_{ex} = k_{off}/(1 - P_B)$ where P_B is the bound ligand fraction. Since our sample conditions are such that P_B is $\ll 1$, we have $k_{ex} \approx k_{off}$. Note that k_{off} reflects the strength of interactions between the ligand and receptor, and its inverse may be regarded as the mean life time for the ligand–receptor complex. A comparison of $k_{ex} \approx k_{off}$ values for a series of ligands to a common receptor therefore allows for a comparison of the relative "tightness" at the respective ligand–receptor interfaces.

If we know the association rate constant k_{on}, then we can estimate the equilibrium dissociation constant, K_D using the ratio $K_D = k_{off}/k_{on} \approx k_{ex}/k_{on}$. An assumption often used in pharmaceutical screens of small molecule ($M_r \leq 500$) libraries against large enzymatic targets ($M_r > 10{,}000$) is that k_{on} is diffusion-controlled. If we assume a k_{on} value of $1 \times 10^9\ M^{-1}\ s^{-1}$, then we get a K_D estimate similar to that obtained by isothermal

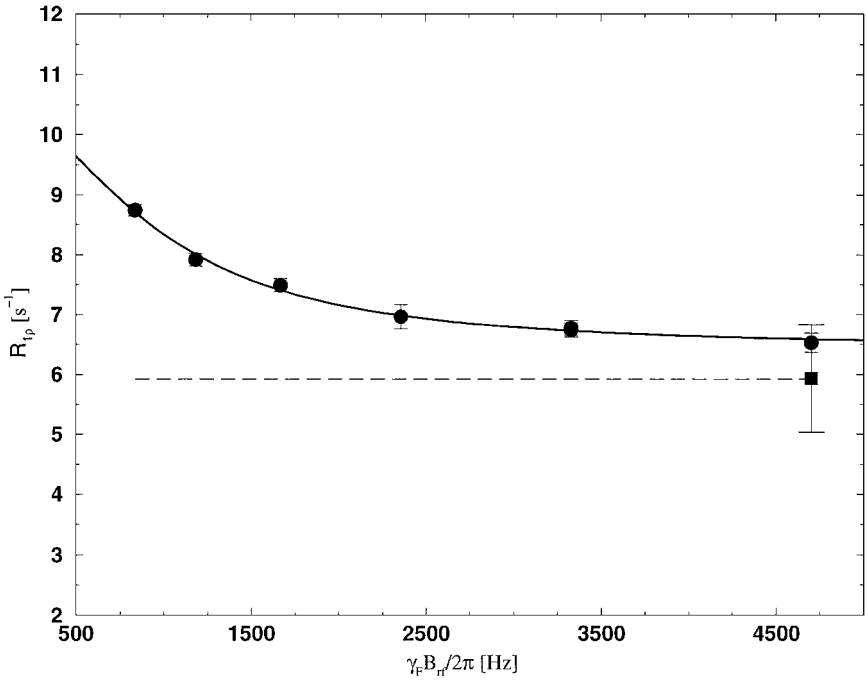

FIG. 7. ^{19}F $R_{1\rho}$ dispersion for the ligand–receptor mixture (ligand at 1 mM, receptor protein at 70 μM). The dotted line is the fitted functional dependence with a corresponding k_{ex} of 5800 $\pm$ 180 s^{-1}. The horizontal line with error bar indicates the nonexchange contribution, $R_2^{NE} = 5.9 \pm 0.9$ s^{-1}, obtained from the quotient of the exchange-averaged cross-relaxation rate, $\eta_{xy,avg}$, and the free compound ratio $|\eta_{xy}/R_2|$.

titration calorimetry (ITC). Specifically, the ratio $k_{ex}/1 \times 10^9$ M^{-1} s^{-1} gives an NMR estimate of $K_D = 5.8 \pm 0.2$ μM while the calorimetry study yields $K_D = 4.8 \pm 0.9$ μM (M. Parker, personal communication, 2001). Thus, the ITC and ^{19}F NMR results are mutually consistent insofar as $k_{on} = 1 \times 10^9$ M^{-1} s^{-1} is reasonable. Simple collision models estimate the upper-limit for a diffusion-controlled k_{on} at room temperature to be $\approx 1 \times 10^{10}$ M^{-1} s^{-1} (*35*, *36*), while typical experimental values for k_{on} are $\approx 1 \times 10^9$ M^{-1} s^{-1} (*37*). Thus, our use of $k_{on} \approx 1 \times 10^9$ M^{-1} s^{-1} is reasonable for the diffusion-controlled encounter between the small compound ($M_r = 242$) under study and the much larger protein target ($M_r \approx 15{,}400$).

IV. DISCUSSION AND CONCLUSIONS

Fluorinated compounds have desirable properties both from a pharmaceutical and spectroscopic standpoint. We have already elaborated on the spectroscopic advantages of ^{19}F NMR. The pharmaceutical advantages include improved pharmacological properties for biologically active compounds (*14*). These factors, along with the growing focus of biological NMR on screening (*28*), have motivated our investigations into fluorine NMR as a tool for characterizing ligand–receptor binding. Often, a simple comparison of the fluorine spectra for a mixture of compounds provides sufficient evidence to expose the binding compounds, or, "hits." The ^{19}F relaxation methods presented here aid efforts to rank-order the affinities of these hits. Such methods include the detection and quantification of the rate constant η_{xy}, which arises from the cross-correlation between the ^{19}F CSA and ^{19}F–^{1}H DD relaxation mechanisms, and mediates cross-relaxation between transverse in-phase and antiphase fluorine magnetization.

We have pointed to several useful properties of η_{xy} from the standpoint of ligand-binding studies. First, η_{xy} has a strong dependence on the overall rotational correlation time of the fluorinated compound. This arises from the secular spectral density contribution $J_u^{CD}(0)$ shown in Eq. [5]. As a consequence, the magnitude of η_{xy} increases with slower molecular tumbling (longer correlation time), and becomes amplified in the bound state. For a mixture of compounds in the presence of a given receptor, we therefore expect an $|\eta_{xy}|$ enhancement for compounds that bind, since they transiently adopt the slow tumbling of the high-molecular-weight receptor. The rate constant η_{xy} therefore has similar utility as the proton R_2 and the ^{1}H–^{1}H NOE in that it acts as a diagnostic of binding.

A second useful property of η_{xy} is its ability to expose chemical exchange contributions to R_2. The dependence of η_{xy} and R_2 on the ^{19}F CSA spectral density functions is quite similar. Under conditions in which the CSA dominates the ^{19}F relaxation, the ratio $|\eta_{xy}/R_2|$ becomes highly insensitive to changes in the overall rotational correlation time, τ_c, of the molecule. This insensitivity translates into high sensitivity to the presence of exchange contributions to R_2. However, R_2 can also be laden with exchange contributions R_{ex} while η_{xy} cannot. Exchange

therefore leads to decreases in the $|\eta_{xy}/R_2|$ ratio. The range of correlation times over which $|\eta_{xy}/R_2|$ is insensitive to τ_c is broader than that of ^{15}N for the same field strength; this is attributed to the greater dominance of the CSA relaxation mechanism in the case of ^{19}F than in the case of ^{15}N.

We note that the above behavior of $|\eta_{xy}/R_2|$ with respect to τ_c and R_{ex} is predicated on the simple proportionality between the cross-correlation spectral density function $J^{CD}_{x,y}(\omega)$, and the auto-correlation spectral densities $J^{DD}(\omega)$ and $J^{CC}(\omega)$. In turn, this proportionality is a convenient consequence of the isotropic rotor spectral density function shown in Eq. [9b]. This is obviously a highly simplified description of the orientational fluctuations experienced by the fluorinated compound. It fails to take into account the possibility of significant internal flexibility of the ligand (smaller S^2 with associated longer internal correlation time), as well as overall anisotropic tumbling of the protein–ligand complex. Additionally, the extent of internal flexibility may change between the free and bound states of the compound. Either of these "real-life" effects will inevitably complicate the relationship between the cross- and auto-correlation spectral densities. However, it is not immediately obvious how significant an effect they would have on the behavior of $|\eta_{xy}/R_2|$ as a function of overall molecular tumbling. We are currently simulating the effects of more exotic spectral density functions to account for the possibilities of large anisotropy in the overall hydrodynamic rotational diffusion, as well as internal flexibility. On the other hand, the prevailing dogma of inhibitor design is to eliminate the internal flexibility of the ligand in order to minimize the entropy losses upon binding. From such a conservative perspective, the effects of internal flexibility in "real" drugs do not elicit great concern or interest.

In typical pharmaceutical settings, NMR is only one of numerous biophysical techniques available for generating and optimizing lead compounds. To maximize the efficiency by which NMR screening data can be integrated with data from other techniques, it is desirable to correlate the NMR screening data with estimates of relative binding affinity. In this context, the ^{19}F η_{xy} experiments are appealing since their measurement along with $R_{1\rho}$ provide a means for rank ordering the tightness of ligand binding under the same conditions as the NMR screen. Rotating frame relaxation measurements ($R_{1\rho}$) have long been used to measure exchange rate constants that then enable estimates of binding affinity parameters such as k_{off} and K_D. However, the accurate extraction of the exchange rate constants relies critically on having a full $R_{1\rho}$ dispersion such that the nonexchange contributions to $R_{1\rho}$ are well characterized by the data. Unfortunately, this can be very difficult or impossible to obtain, and the lack of an *a priori* estimate of the nonexchange contributions leads to erroneous exchange rates. The $|\eta_{xy}/R_2|$ ratio provides a convenient remedy. If the ratio $|\eta_{xy}/R_2|$ for the free ligand is exempt from R_{ex} effects, then the crucial nonexchange contributions to $R_{1\rho}$ can be estimated from the quotient of the excahnge-averaged η_{xy} and the free state ratio. Thus, the $|\eta_{xy}/R_2|$ measurements improve the accuracy of exchange rate constants that can be obtained from the $R_{1\rho}$ measurements, and thus provide for more accurate estimates of the dissociation rate constant k_{off}. In lieu of $R_{1\rho}$ measurements, the ratio allows one to estimate the R_{ex} exchange contribution to an R_2 measurement. A comparison of these exchange contributions for a series of related ligands may therefore help rank order their corresponding affinities.

In principal, equilibrium dissociation constants K_D can be obtained by observing changes in NMR relaxation parameters (e.g., R_1, R_2, transferred NOE, ROE) during the course of a titration. However, within the confines of pharmaceutical NMR screening protocols, such titrations are not always practical. For example, ligand titrations often require the persistent addition of compounds dissolved in organic solvents hostile to the integrity of the protein. Additionally, protein titrations can lead to aggregation at the higher concentrations needed for characterizing weaker binders. Finally, titrations involving relaxation measurements can seriously decrease throughput since a relaxation series must be performed for each ligand or protein concentration. From this viewpoint, the k_{off} values provided by the η_{xy} and $R_{1\rho}$ measurements are attractive since they comprise a "titrationless" means for extracting binding affinity information.

It should be noted that translational diffusion measurements for ligands via pulsed field gradient experiments offer an alternative "titrationless" means for estimating binding affinity. A distinct advantage of diffusion methods is that K_D can be determined directly, as opposed to k_{off} (*28*, *38*). The disadvantage of diffusion methods is the decrease in experimental sensitivity. Specifically, in the fast-exchange regime, we observe the population-weighted average of the bound and free ligand diffusion coefficients. However, the bound ligand diffusion coefficient is smaller than the free ligand diffusion coefficient. Thus, to detect binding, we must work with nearly equimolar amounts of ligand and receptor (see, e.g., results in (*1*, *28*)). These conditions contrast with the large ligand excesses typical of NMR screening. If the receptor concentration is limited (e.g., because of poor solubility or expression), then correspondingly low ligand concentrations are called for, and the sensitivity of the experiment suffers. Additionally, the popular diffusion experiments use the stimulated echo, which refocuses only half of the original coherence (see, e.g., (*39*)), thus further compromising sensitivity. Note that the bound state reduction of the translational diffusion coefficient contrasts sharply with the bound state enhancement of η_{xy} and $R_{1\rho}$. The latter enhancement is of course what allows us to observe binding effects even in the presence of large ligand excess.

By itself, k_{off} provides information about the tightness by which a given receptor binds a ligand. A comparison of k_{off} values for a set of ligands to the same receptor provides insight into the strength of intermolecular interactions at the receptor–ligand interface. To go further and estimate K_D, we need the ratio k_{off}/k_{on}. The ligand-based NMR screening protocols use a large ligand excess because they detect binding via perturbations in

the ligand NMR spectral parameters (*1*). Due to this excess, the k_{ex} values from the ^{19}F relaxation measurements essentially give us k_{off}. In contrast, k_{on} must be obtained by other means. For the present study, the assumption of $k_{on} = 1 \times 10^9$ M^{-1} s^{-1} leads to an estimated K_D that is consistent with the K_D obtained from isothermal-titration calorimetry. The assumed value lies within the range of k_{on} values reasonable for a diffusion-controlled reaction between the small ligand ($M_r = 242$) and the much larger target molecule ($M_r = 15{,}400$) (*37*). In general, however, k_{on} may be considerably slower than that appropriate for diffusion-controlled encounters due to presence of activation energy barriers or multistep binding. Even within the confines of diffusion-controlled binding, k_{on} can still span several orders of magnitude due to electrostatic or conformational gating effects (*36*). Without additional measurements for determining k_{on}, the K_D estimates are obviously vulnerable to the potential errors inherent in the k_{on} assumptions. Nonetheless, these uncertainties need not destroy our ability to rank order ligand-binding affinities via the ^{19}F relaxation measurements. In particular, if the variation in k_{off} is much stronger than the variation in k_{on} then a rank-ordering of k_{off} yields an accurate rank-ordering of K_D. Such can be the case if we consider a series of ligands belonging to the same enzyme target. Alternatively, we may choose to articulate the ligand-binding mechanism, and compare k_{on} values for a ligand series. This is possible if K_D values are already known from independent measurements. We can then estimate the k_{on} rate constant from K_D/k_{off}. Clearly, this value should not exceed what is reasonable for a diffusion-limited k_{on}.

We have presented pulse sequences that demonstrate the ^{19}F CSA-DD cross-correlation effect via ^{19}F and ^{1}H chemical shifts correlation spectra. Such sequences exploit the cross-correlated cross-relaxation pathway $F_{xy} \leftrightarrow 2I_zF_{xy}$ to achieve polarization transfer between fluorine and proton. The use of CSA-DD cross-correlation for polarization transfer has recently been analyzed in detail for protein amide ^{15}N–^{1}H spin systems by Riek *et al.* (*21*). Analogous approaches might also be advantageous for fluorinated compounds. In particular, for the aromatic fluorine moiety examined here, the heteronuclear scalar coupling constants are small. As the overall molecular tumbling time increases, the transverse auto-relaxation rate constants increase while the scalar coupling constants remain fixed; these trends lead to decreasing efficiency of INEPT-style polarization transfer methods. In contrast, the magnitude of η_{xy} increases with molecular weight, and may therefore prove more efficient for fluorine–proton polarization transfer in slowly tumbling compounds.

The increase of η_{xy} with B_o and molecular size depicted in Fig. 2A leads one to consider possible advantages of TROSY pulse sequence methods (*20*) in ^{19}F spectroscopy. In the TROSY approach, one exploits the aforementioned differential transverse relaxation by observing only the slowest relaxing component of the chosen multiplet. For ^{15}N-enriched proteins having large rotational correlation times, this has led to dramatic gains in sensitivity and resolution. Optimal TROSY conditions are those for which the interaction strengths of the CSA and DD mechanisms cancel one another. This requires that the CSA constant C_{uu} of Eq. [7] be of magnitude similar to that of d_{FH} of Eq. [8]. Cancellation also requires that the ^{19}F CSA tensor be axially symmetric, with the symmetry axis collinear with the DD interaction vector, $\mathbf{r}_{FH}$. Unfortunately, the ^{19}F–^{1}H spin system under consideration falls short of these criteria due to the disparity between the DD and CSA interaction strengths and the asymmetry of the ^{19}F CSA tensor. An additional hindrance is the small scalar J_{FH} coupling constant in the aromatic ring. TROSY pulse schemes use a number of spin-echo sandwiches to achieve the correct multiplet selection. For the aromatic fluorine, the analogous spin echoes would entail delays of ≈30–40 ms, thus turning TROSY into an effective but unwanted relaxation filter. To achieve TROSY gains, we need to increase the contribution of the DD relaxation relative to the CSA relaxation. This can be achieved by working at lower B_o. Use of Eqs. [7] and [8] show that a B_o corresponding to a ^{1}H resonance frequency of ≈136 MHz would be ideal. Alternatively, one can also study ^{19}F–^{1}H spin systems with shorter r_{FH} distances. Equations [7] and [8] indicate that the r_{FH} distance of ≈ 1.8 Å would elicit significant TROSY gains at the B_o used in this study (11.7 T). Thus, molecules containing geminal ^{19}F–^{1}H spin pairs would be much more promising TROSY candidates than the aromatic spin pair considered here.

We have also proposed pulse sequences to measure the transverse cross-correlation rate constant η_{xy}. The small scalar coupling constants J_{FH} precludes the use of methods designed for ^{15}N-enriched proteins; we have therefore tried a different approach in which we measure the transverse relaxation rate constants of individual quartet members. In our analysis of the η_{xy} data, we have omitted the effects of proton–proton cross-relaxation that can ensue between the transverse magnetizations of the various quartet members. This cross-relaxation intensifies in proportion to the local proton density of the protons that have significant dipolar coupling to the fluorine. At present, the pulse sequences have initial conditions such that only the desired quartet member is excited. This reduces but does not eliminate the cross-relaxation effects, and improved techniques are under study.

We note that the $R_{1\rho}$ rate constants obtained via the simple CW pulse scheme are partially corrupted by the η_{xy} cross-relaxation during the spin lock, leading to erroneously shorter rate constants. Unfortunately, the hardware did not permit simultaneous ^{19}F and ^{1}H pulsing, and we were therefore unable to quench the CSA-DD cross-relaxation via the compensatory ^{1}H 180°'s used in the CPMG sequences (*16*, *34*). However, in practice, the correct rate constants differ only by ≈5% from the measured rate constants, and therefore, the error is not severe. This was verified by comparing the difference in compensated CPMG R_2 with the "uncompensated" $R_{1\rho}$ for the free ligand at 10, 14, and 22°C. Such small differences are not expected to alter significantly the $R_{1\rho}$ dispersion and the conclusions drawn thereof.

The use of adiabatic spin locks (*40, 41*) may help mitigate these complications, as well as those arising from resonance offset effects incurred by the use of low rf field strengths that are $\leq|\delta_F - \delta_B|$ (*3, 42*). Such studies are in progress.

Although the studies here have focused on exchange processes associated with binding, the methods presented could be conceivably expanded to describe other exchange processes. For example, internal ligand flexibility on the micro- to millisecond time scale might also be of interest. Also, given the advent of cold probes, the methods presented here are conceivably transferable to aromatic ^{13}C nuclei. Investigations along these lines are in progress.

V. EXPERIMENTAL

Primarily two samples were used in this study: one consisting of the free ligand at 1 mM, and another containing 1 mM ligand in the presence of 70 μM protein. Both molecules were dissolved in a D_2O buffer containing 100 mM phosphate and 1 mM DTT (pH 7.0, uncorrected). Measurements were performed at 11.7 T on a Bruker DRX system equipped with a QNP probe and a single-axis gradient. Additional samples included the free ligand mixed with 50% v/v deutero-glycerol (Isotec, Inc.), dissolved in the same buffer described above. For the protein–ligand interaction studies, the temperature was fixed at 22°C. Additional relaxation measurements on the free compound codissolved with glycerol were performed at 22, 14, and 10°C.

Fluorine R_2 measurements used a compensated CPMG sequence (*16, 34*). Successive ^{19}F 180° pulses were separated by 5 ms. Relaxation delays included 20.2, 40.4, 60.6, 80.8, 101.0, 121.2, 141.4, 161.6, and 181.8 ms. On-resonance fluorine $R_{1\rho}$ measurements used a simple CW spin lock in the sequence $90^\circ(F)_y$–(Spin lock)$_{\pm x}$–Detect. The spin lock strengths were calibrated by measuring the residual ^{19}F–^1H scalar coupling (proton I, Fig. 1) in the proton spectrum as a function of the ^{19}F CW decoupling carrier offset. For the measurements in glycerol, the spin lock lengths were matched to the CPMG delays given above. For the fluorine $R_{1\rho}$ dispersion study on the ligand–protein sample, a series of $R_{1\rho}$ measurements was conducted at seven spin lock strengths including 4701, 3328 (x2), 2356, 1668, 1181, and 836 Hz. Each field strength included 14 spin lock lengths of 8(x2), 12, 26, 35, 48, 60, 70(x2), 80, 90, 100, 114(x2) ms. Measurements of η_{xy} were carried out using the pulse scheme of Fig. 4c. Measurements used 14 spin lock delays including 10(x2), 15, 20(x2), 25, 30, 40, 50, 60, 70, 80, 90, 100 ms and a B_1 field of 4.3 kHz. All relaxation spectra used 128 transients per relaxation delay, resulting in 7.5 min per 1D spectrum.

Relaxation rate constants were estimated by a two-parameter fit of the 1D peak intensities to the single exponential $A^* \exp(-RT)$ using the Levenburg–Marquardt algorithm for nonlinear least squares fitting (*43*). Statistical errors in the fitted rate constants amplitude factor, A, and the relaxation rate constant R were estimated using standard Monte Carlo methods (see, e.g., (*44*)). Statistical errors in the ratio $|\eta_{xy}/R_2|$ were estimated using standard error propagation rules. The $R_{1\rho}$ dispersion data were fitted using the offset Lorentzian function of Eq. [14]. Initial values for the constants A, k_{ex}, and R_2^{NE} were obtained by fixing R_2^{NE} at the value predicted by the cross-correlation measurements and allowing A and k_{ex} to vary in a simple grid search (*43*). These results were then used as initial conditions for the Levenburg–Marquardt algorithm, in which all three parameters were allowed to vary. Final errors were estimated using the aforementioned Monte Carlo methods.

ACKNOWLEDGMENTS

The author is grateful to Jasna Fejzo, Jon Moore, Cheryl Schairer, Prof. Jonathan Lee, Brian Hare, Scott Raybuck, Martyn Botfield, Matt Parker, Mark Namchuk, Dave Pearlman, Chris Lepre, and Paul Charifson for reading of the manuscript and/or stimulating discussions. The author is indebted to Matt Parker for the isothermal titration calorimetry study. The author further expresses gratitude to Norzehan Abdul-Manan for availability of the protein. This paper is dedicated to Professor Jean-Francois Lefevre.

REFERENCES

1. J. W. Peng, C. A. Lepre, J. Fejzo, N. Abdul-Manan, and J. M. Moore, Nuclear magnetic resonance-based approaches for lead generation in drug discovery, *in* "Methods in Enzymology" (T. L. James, V. Dötsch, and N. J. Oppenheimer, Eds.), pp. 202–230, Academic Press, San Diego (2001).
2. J. T. Gerig, Fluorine NMR of proteins, *Prog. Nucl. Magn. Reson. Spectrosc.* **26,** 293–370 (1994).
3. D. G. Davis, M. E. Perlman, and R. E. London, Direct measurements of the dissociation-rate constant for inhibitor-enzyme complexes via the $T_{1\rho}$ and T_2(CPMG) methods, *J. Magn. Reson. Ser. B* **104,** 266–275 (1994).
4. C. Deverell, R. E. Morgan, and J. H. Strange, Studies of chemical exchange by nuclear magnetic relaxation in the rotating frame, *Mol. Phys.* **18,** 553–559 (1970).
5. Z. Y. Peng, N. Tjandra, V. Simplaceanu, and C. Ho, Slow motions in oriented phospholipid bilayers and effects of cholesterol or gramicidin, *Biophys. J.* **56,** 877–885 (1989).
6. D. P. Cistola and K. B. Hall, Probing internal water molecules in proteins using two-dimensional 19F-1H NMR *J. Biolmol. NMR* **5,** 415–419 (1995).
7. R. E. London and S. A. Gabel, Fluorine-19 NMR studies of fluorobenzeneboronic acids. 1. Interaction kinetics with biologically significant ligands, *J. Am. Chem. Soc.* **116,** 2562–2569 (1994).
8. R. E. London and S. A. Gabel, Fluorine-19 NMR studies of fluorobenzeneboronic acids. 2. Kinetic characterization of the interaction with subtilisin Carlsberg and model ligands, *J. Am. Chem. Soc.* **116,** 2570–2575 (1994).
9. L. A. Luck, J. E. Vance, T. M. O'Connell, and R. E. London, ^{19}F NMR relaxation studies on 5-fluorotryptophan- and tetradeutero-5-fluorotryptophan-labeled E. coli gulcose/galactose receptor, *J. Biomol. NMR* **7,** 261–272 (1996).
10. D. L. Tierney, G. T. Gassner, C. Luchinat, I. Bertini, D. P. Ballou, and J. E. Penner-Hahn, NMR characterization of substrate binding in the phthalate dioxygenase system, *Biochemistry* **38,** 11,051–11,061 (1999).
11. E. L. Mackor and C. MacLean, Sign of JHF in CHFC12, *J. Chem. Phys.* **44,** 64–69 (1966).
12. S. G. Withers, N. B. Madsen, and B. D. Sykes, Relaxation of individual transitions in an AX spectrum. Use of interference terms to separate the dipolar and chemical-shift anisotropy contributions to the relaxation of ^{31}P and ^{19}F nuclei in macromolecules, *J. Magn. Reson.* **61,** 545–549 (1985).

13. R. C. R. Grace and A. Kumar, Observation of cross correlations in a weakly coupled 19F-1H four-spin system, *J. Magn. Reson. Ser. A* **115,** 87–93 (1995).
14. B. Wakefield, Fluorinated pharmaceuticals, *Innov. Pharm. Technol*. 74–78 (2000).
15. J. Boyd, U. Hommel, and I. D. Campbell, Influence of cross-correlation between dipolar and anisotropic chemical shift relaxation mechanisms upon longitudinal relaxation rates of ^{15}N in macromolecules, *Chem. Phys. Lett.* **175,** 477–482 (1990).
16. A. G. Palmer III, N. J. Skelton, W. J. Chazin, P. E. Wright, and M. Rance, Suppression of the effects of cross-correlation between dipolar and anisotropic chemical shift relaxation mechanisms in the measurement of spin-spin relaxation rates, *Mol. Phys.* **75,** 699–711 (1992).
17. M. Goldman, Interference effects in the relaxation of a pair of unlike spin-1/2 nuclei, *J. Magn. Reson.* **60,** 437–452 (1984).
18. C. D. Kroenke, J. P. Loria, L. K. Lee, M. Rance, and A. G. Palmer III, Longitudinal and transverse ^{1}H-^{15}N dipolar/^{15}N chemical shift anisotropy relaxation inteference: Unambiguous determination of rotational diffusion tensors and chemical exchange effects in biological macromolecules, *J. Am. Chem. Soc*. **120,** 7905–7915 (1998).
19. N. Tjandra, A. Szabo, and A. Bax, Protein backbone dynamics and 15N chemical shift anisotropy from quantitative measurement of relaxation interference effects, *J. Am. Chem. Soc.* **118,** 6986–6991 (1996).
20. K. Pervushin, R. Riek, G. Wider, and K. Wüthrich, Attenuated T_2 relaxation by mutual cancellation of dipole-dipole coupling and chemical shift anisotropy indicates an avenue to NMR structures of very large biological macromolecules in solution, *Proc. Natl. Acad. Sci. USA* **94,** 12,366–12,371 (1997).
21. R. Riek, G. Wider, K. Pervushin, and K. Wüthrich, Polarization transfer by cross-correlated relaxation in solution NMR with very large molecules, *Proc. Natl. Acad. Sci. USA* **96,** 4918–4923 (1999).
22. J. Keeler and F. Sanchez-Ferrando, The influence of cross correlation on multiplet patterns in nuclear Overhauser effect spectra, *J. Magn. Reson.* **75,** 96–109 (1987).
23. Y. Hiyama, J. V. Silverton, D. A. Torchia, J. T. Gerig, and S. J. Hammond, Molecular structure and dynamics of crystalline p-fluoro-D-L-phenylalanine. A combined X-ray/NMR investigation, *J. Am. Chem. Soc.* **108,** 2715–2723 (1986).
24. G. Lipari and A. Szabo, Model-free approach to the interpretation of nuclear magnetic resonance relaxation in macromolecules, *J. Am. Chem. Soc.* **104,** 4546–4559 (1982).
25. A. G. Palmer III, J. Williams, and A. McDermott, Nuclear magnetic resonance studies of biopolymer dynamics, *J. Phys. Chem.* **100,** 13,293–13,310 (1996).
26. B. Brutscher, R. Brüschweiler, and R. R. Ernst, Backbone dynamics and structural characterization of the partially folded a state of ubiquitin by ^{1}H, ^{13}C, and ^{15}N nuclear magnetic resonance spectroscopy, *Biochemistry* **36,** 13,043–13,053 (1997).
27. D. Fushman and D. Cowburn, Model-independent analysis of 15N chemical shift anisotropy from NMR relaxation data. Ubiquitin as a test example, *J. Am. Chem. Soc.* **120,** 7109–7110 (1998).
28. J. Fejzo, C. A. Lepre, J. W. Peng, G. W. Bemis, Ajay, M. A. Murcko, and J. M. Moore, The SHAPES strategy: An NMR-based approach for lead generation in drug discovery, *Chem. Biol*. **6,** 755–769 (1999).
29. H. Wennerström, Nuclear magnetic relaxation induced by chemical exchange, *Mol. Phys.* **24,** 69–80 (1972).
30. G. A. Morris and R. Freeman, Enhancement of nuclear magnetic resonance signals by polarization transfer, *J. Am. Chem. Soc.* **101,** 760–762 (1979).
31. T. L. Hwang and A. J. Shaka, Water suppression that works. Excitation sculpting using arbitrary waveforms and pulsed field gradients, *J. Magn. Reson. Ser. A* **112,** 275–279 (1995).
32. K. Pervushin, R. Riek, G. Wider, and K. Wüthrich, Transverse relaxation-optimized spectroscopy (TROSY) for NMR studies of aromatic spin systems in ^{13}C-labeled proteins, *J. Am. Chem. Soc.* **120,** 6394–6400 (1998).
33. R. R. Ernst, G. Bodenhausen, and A. Wokaun, "Principles of Magnetic Resonance in One and Two Dimensions," Oxford Univ. Press, Oxford (1990).
34. L. E. Kay, L. K. Nicholson, F. Delaglio, A. Bax, and D. A. Torchia, Pulse sequences for removal of the effects of cross correlation between dipolar and chemical-shift anisotropy relaxation mechanisms on the measurement of heteronuclear T1 and T2 values in proteins, *J. Magn. Reson.* **97,** 359–375 (1992).
35. C. R. Cantor and P. R. Schimmel, "Biophysical Chemistry, Part III: The Behavior of Biological Macromolecules," W. H. Freeman, New York (1980).
36. J. A. McCammon and S. C. Harvey, "Dynamics of Proteins and Nucleic Acids," Cambridge Univ. Press, Cambridge (1988).
37. A. Fersht, "Enzyme Structure and Mechanism," 2nd ed., W. H. Freeman, New York (1985).
38. D. J. Detlefsen, F. Xu, S. E. Hill, and M. E. Hail, A new gear for nuclear magnetic resonance in pharmaceutical research, *Am. Pharm. Rev.* **3,** 43 (2000).
39. D. Wu, A. Chen, and C. S. Johnson Jr., An improved diffusion-ordered spectroscopy experiment incorporating bipolar-gradient pulses, *J. Magn. Reson. Ser. A* **115,** 260–264 (1995).
40. H. Desvaux, Improved versions of off-resonance ROESY, *J. Magn. Reson. Ser. A* **113,** 47–52 (1995).
41. F. A. A. Mulder, R. A. de Graaf, R. Kaptein, and R. Boelens, An off-resonance rotating frame relaxation experiment for the investigation of macromolecular dynamics using adiabatic rotations, *J. Magn. Reson.* **131,** 351–357 (1998).
42. M. Akke and A. G. Palmer III, Monitoring macromolecular motions on the microsecond to millisecond time scales by $R_{1\rho}$-R_1 constant relaxation time NMR spectroscopy, *J. Am. Chem. Soc.* **118,** 911–912 (1996).
43. W. H. Press, S. A. Teukolsky, W. T. Vetterling, and B. P. Flannery, "Numerical Recipes in C. The Art of Scientific Computing," 2nd ed., Cambridge Univ. Press, Cambridge (1992).
44. J. W. Peng and G. Wagner, Frequency spectrum of NH bonds in eglin C from spectral density mapping at multiple fields, *Biochemistry* **34,** 16,733–16,752 (1995).